JOURNAL OF SOLID STATE CHEMISTRY 110, 337–344 (1994)

New Quaternary Chalcogenides Ba*LnMQ*$_3$ (*Ln* = Rare Earth or Sc; *M* = Cu, Ag; *Q* = S, Se)

II. Structure and Property Variation vs Rare-Earth Element

Ping Wu, Amy E. Christuk, and James A. Ibers

Department of Chemistry, Northwestern University, Evanston, Illinois 60208-3113

Received June 7, 1993; in revised form August 16, 1993; accepted August 17, 1993

Some new quaternary compounds of the type Ba*LnMQ*$_3$ (*Ln* = rare earth or Sc; *M* = Cu, Ag; *Q* = S, Se) have been synthesized by the reaction of the constituent binary chalcogenides and elements at 1000°C. The crystal structures of two of these compounds have been determined by single-crystal X-ray diffraction techniques and are isostructural. Crystal data: $BaErCuS_3$—space group D_{2h}^{17}—*Cmcm*, $M = 464.32$, $Z = 4$, $a = 3.987(1)$, $b = 13.377(3)$, $c = 10.101(2)$ Å ($T = 115$ K), $V = 538.7(4)$ Å^3, $R_w(F^2) = 0.095$ for 848 observations and 24 variables, $R(F) = 0.037$ for 840 observations having $F_o^2 > 2\sigma(F_o^2)$; $BaYAgSe_3$—space group D_{2h}^{17}—*Cmcm*, $M = 571.0$, $Z = 4$, $a = 4.239(1)$, $b = 14.030(2)$, $c = 10.636(2)$ Å ($T = 115$ K), $V = 632.6(2)$ Å^3, $R_w(F^2) = 0.057$ for 645 observations and 24 variables, $R(F) = 0.023$ for 595 observations having $F_o^2 > 2\sigma(F_o^2)$. These two compounds adopt the layered $KZrCuS_3$ structure type. The layers, which are separated by Ba^{2+} ions, consist of edge-sharing octahedral chains and corner-sharing tetrahedral chains. The other compounds synthesized crystallize either with this same structure or with that of β-$BaLaCuSe_3$, a slightly distorted variation, which is isostructural with Eu_2CuS_3. The diffuse reflective UV-visible spectra of several of these compounds have been measured. From magnetic susceptibility measurements, both $BaNdCuS_3$ and $BaGdCuS_3$ show Curie–Weiss behavior, whereas $BaCeCuS_3$ and $BaCeCuSe_3$ show in addition *temperature-independent paramagnetism.*

INTRODUCTION

Many binary and ternary chalcogenides containing rare-earth elements are known (1, 2). They adopt a wide range of structure types and they display a variety of interesting physical properties (1). These materials have potential applications, for example, as luminescent materials (3) and infrared windows (4). Because of the similarity in chemical composition of these systems to some of the high-temperature superconducting cuprates, efforts have been made to synthesize sulfide analogues of the cuprates (5, 6). While ternary chalcogenides containing a rare-earth element and another metal are known, relatively few quaternary chalcogenides containing a rare-earth element and two other metals are known. Flahaut reviewed three groups of such compounds, with structure types La $CaAl_3S_7$, $La_6Cu_2Si_2S_{14}$, and $La_2Sr_3Sn_3S_{12}$ (1). More recently, Ibanez *et al.* synthesized $NaNdGa_4S_8$ (7), which crystallizes in a derivative of the $EuGa_2S_4$ structure type, and Carpenter and Hwu synthesized $CaYbInQ_4$ (*Q* = S, Se) (8), which crystallizes in the Mg_2SiO_4 structure type.

Recently, several series of quaternary chalcogenides have been synthesized in this laboratory (9–14). These studies have been extended to the rare-earth systems in which we have found new structural features (15). Here we describe the synthesis and characterization of a new series of quaternary chalcogenides Ba*LnMQ*$_3$ (*Ln* = Ce, Nd, Gd, Y, Er, or Sc; *M* = Cu, Ag; *Q* = S, Se).

EXPERIMENTAL

Syntheses. Several compounds of formula Ba*LnMQ*$_3$ (*Ln* = rare earth or Sc; *M* = Cu, Ag; *Q* = S, Se) were prepared by the reaction of elemental Cu or Ag (both AESAR, 99.999%) and S (Alfa, 99.9995%) or Se (Aldrich, 99.999%) with binary chalcogenides BaS (AESAR, 99.9%) or BaSe (prepared from the high-temperature stoichiometric reaction of Ba (AESAR, 99.5%) and Se) and Ln_2Q_3 (La_2S_3 from Strem, 99.9%, the rest prepared by high-temperature reactions of the metals (all from Johnson Matthey, 99.9%) with S or Se). The starting materials were placed in quartz tubes that were subsequently evacuated to 10^{-5} Torr and sealed. After a preliminary study, an elemental ratio of 1 : 1 : 1 : 3 for Ba : *Ln* : *M* : *Q* was used. The quartz tubes were heated gradually to 500°C where they were kept for 24 hr before being successively brought to 700°C for 24 hr and 1000°C for 150 hr. The tubes were then cooled at a rate of 4°C/hr to 300°C and then the furnace was shut off. In each system the crystals that had grown in the tubes were analyzed semiquantitatively by EDAX with the microprobe of a Hitachi S-570 scanning

0022-4596/94 $6.00

electron microscope. The presence of all four elements in these crystals was confirmed; in most systems a ratio of approximately 1 : 1 : 1 : 3 was found, but for crystals of several compounds a ratio of approximately 2 : 1 : 5 : 6 was also found. All of these compounds are modestly stable in air and water.

An alternative synthetic route involving halide fluxes was used to grow some of the single crystals of $BaCeCuSe_3$, $BaErCuSe_3$, $BaYCuSe_3$, $BaErAgSe_3$, and $BaYAgSe_3$. The starting material consisted of a mixture of $BaBr_2$ (AESAR, 99.9%, dried at 400°C for 12 hr), the rare-earth element, Cu or Ag, K_2Se_3 (prepared from the stoichiometric reaction of elemental K (AESAR, 99%) and Se in liquid ammonia under an atmosphere of argon), and KBr (Strem, 99.999%). The same experimental procedure previously described (15) was used. EDAX experiments confirmed the stoichiometry of these compounds.

Bulk samples of the various compounds were prepared by reactions of stoichiometric amounts of starting materials at 850°C for 6 days. One or two intermittent grindings were necessary.

Crystallographic study of $BaErCuS_3$. A needle-like crystal of approximate dimensions 0.05 by 0.05 by 0.10 mm was selected for data collection. Intensity data were collected by the θ–2θ scan technique on a Picker diffractomer (16). The lattice constants were determined from a least-squares analysis of the setting angles of 25 reflections in the range $35° < 2\theta$ (Mo$K\alpha_1$) $< 44°$ that had been automatically centered at 115 K. The refined cell constants and additional relevant crystal data are given in Table 1. Six standard reflections measured every 100 reflections throughout data collection showed no significant variations in intensity.

The initial data processing was carried out on a Stardent computer with programs and methods standard in this laboratory. From the systematic absences, the space groups $Cmcm$, $Cmc2_1$, or $C2cm$ were possible. The data were corrected for absorption and averaged in Laue sym-

TABLE 1
Crystal Data and Experimental Details for $BaErCuS_3$ and $BaYAgSe_3$

Compound	$BaErCuS_3$	$BaYAgSe_3$
Formula weight	464.32	571.0
Space group	D_{2h}^{17}—$Cmcm$	D_{2h}^{17}—$Cmcm$
a (Å)	3.987(1)	4.239(1)
b (Å)	13.377(3)	14.030(2)
c (Å)	10.101(2)	10.636(2)
V (Å^3)	538.7(2)	632.6(2)
Z	4	4
T (K)	115[a]	115[a]
Crystal vol. (mm^3)	2.4×10^{-4}	1.6×10^{-4}
Crystal shape	Needle, bounded by (001), (130), ($\bar{1}30$), (01$\bar{1}$), (0$\bar{1}\bar{1}$), (021), (0$\bar{2}$1)	Needle, bounded by {100}, {010}, {001}
Radiation	Graphite monochromated Mo$K\alpha$ ($\lambda(K\alpha_1)$ = 0.7093 Å)	Graphite monochromated Mo$K\alpha$ ($\lambda(K\alpha_1)$ = 0.7093 Å)
Linear abs. coeff. (cm^{-1})	275.7	354.4
Transmission factors[b]	0.278–0.380	0.279–0.398
Detector aperture (mm)	Horizontal, 4.6; vertical, 5.4; 32 cm from crystal	Horizontal, 5.0; vertical, 5.0; 32 cm from crystal
Take-off angle (deg.)	2.5	2.5
Scan speed (deg. min^{-1})	3.0 in 2θ	3.5° ≤ 2θ ≤ 50°, 3.0 in 2θ; 50° ≤ 2θ ≤ 64°, 2.0 in 2θ
Scan type	θ–2θ	θ–2θ
Scan range (deg.)	0.9° below $K\alpha_1$ to 1.3° above $K\alpha_2$	0.6° below $K\alpha_1$ to 0.7° above $K\alpha_2$
λ^{-1} sin θ, limits (Å)	0.0615–0.8680 $5° \le 2\theta$(Mo$K\alpha_1$) $\le 76°$	0.0615–0.7471 $5° \le 2\theta$(Mo$K\alpha_1$) $\le 64°$
Background counts	7 sec at each end of the scan	5° ≤ 2θ ≤ 50°, 5.0 sec; 50° ≤ 2θ ≤ 64°, 9.0 sec at each end of the scan
Data collected	$\pm h \pm k \pm l$	$\pm h \pm k \pm l$
No. of unique data including $F_o^2 < 0$	848	645
No. of unique data with $F_o^2 > 2\sigma(F_o^2)$	840	595
No. of variables	24	24
R_w (F^2)[c]	0.095	0.057
R [on F for $F_o^2 > 2\sigma(F_o^2)$]	0.037	0.023
Error in observation of unit weight	1.81	1.009

[a] The low-temperature system for the Picker diffractometer is based on a design by Huffman (30).
[b] The analytical method was used for the absorption correction (31).
[c] $w^{-1} = \sigma^2(F_o^2) + (0.04 \times F_o^2)^2$ for $F_o^2 \ge 0$ and $w^{-1} = \sigma^2(F_o^2)$ for $F_o^2 < 0$.

metry mmm. The residual for averaging of 3.3% suggests that this is the correct Laue group and hence that the space group is *Cmcm*. Indeed, with the direct methods program SHELXS (17) a solution was found in this space group. The final anisotropic refinement on F_o^2 employed all of the unique data (18). Values of the resultant R indices are 0.095 for $R_w(F^2)$ (all data) and 0.037 for $R(F)$ ($F_o^2 > 2\sigma(F_o^2)$). The highest residual electron density peak has a height about 0.7% that of an Er atom.

Crystallographic study of $BaYAgSe_3$. A needle-like crystal of approximate dimensions 0.03 by 0.03 by 0.16 mm was selected for data collection. Intensity data were collected by the θ–2θ scan technique on a Picker diffractometer. The lattice constants were determined from a least-squares analysis of the setting angles of 52 reflections in the range $35° < 2\theta$ (Mo$K\alpha_1$) $< 40°$ that had been automatically centered at 115 K. The refined cell constants and additional relevant crystal data are given in Table 1. Six standard reflections measured every 100 reflections throughout data collection showed no significant variations in intensity. Systematic absences were again consistent with space groups *Cmcm*, *Cmc*2_1, or *C*2*cm* of the orthorhombic system. The data were corrected for absorption and then averaged in Laue symmetry mmm. The residual for averaging is 4.6%, again consistent with this Laue symmetry and with space group *Cmcm*. We assumed that $BaYAgSe_3$ and $BaErCuS_3$ are isostructural and hence the parameters for the sulfide were the starting point for the refinement of the selenide. The final anisotropic refinement on F_o^2 resulted in values of 0.057 for $R_w(F^2)$ (all data) and 0.023 for $R(F)$ ($F_o^2 > 2\sigma(F_o^2)$). The highest residual electron density has a height of about 0.6% that of a Ba atom.

No unusual trends were found in either structure in an analysis of the goodness of fit as a function of F_o or scattering angle. Final values of the atomic parameters and equivalent isotropic displacement parameters for both compounds appear in Table 2. Final displacement parameters and structure amplitudes are given in Tables 3[1] and 4.[1] The program package SHELXTL PC (17) was used for the ensuing molecular graphics generation.

X-ray powder diffraction and unit cell measurements. For phase identification X-ray powder diffraction patterns of bulk samples were taken on a Philips powder diffractometer. For unit cell determinations, powder diffraction patterns of several members of this series were taken on a Scintag XDS 2000 diffractometer at room temperature. The unit cells were determined by least-squares refinement of uniquely indexed reflections in the range $10° \leq 2\theta < 80°$. Unit cells of several other compounds were determined on single crystals either from Weissenberg or precession photographs taken at room temperature or from least-squares analysis of the setting angles of reflections automatically centered on a CAD4 diffractometer at 115 K.

TABLE 2
Positional Parameters and Equivalent Displacement Parameters

Atom	x	y	z	U_{eq}[a] (Å^3)	Wyckoff position
			$BaErCuS_3$		
Ba	0	0.25566(4)	1/4	0.0053(2)	4*c*
Er	0	0	0	0.0037(2)	4*a*
Cu	0	0.53253(9)	1/4	0.0058(5)	4*c*
S(1)	0	0.63246(12)	0.0599(2)	0.0046(6)	8*f*
S(2)	0	0.0663(2)	3/4	0.0052(9)	4*c*
			$BaYAgSe_3$		
Ba	0	0.24967(3)	1/4	0.0062(2)	4*c*
Y	0	0	0	0.0051(3)	4*a*
Ag	0	0.53155(4)	1/4	0.0068(3)	4*c*
Se(1)	0	0.63717(4)	0.04913(5)	0.0055(2)	8*f*
Se(2)	0	0.07874(5)	3/4	0.0052(3)	4*c*

[a] $U_{eq} = (1/3)\,\Sigma_i\,\Sigma_j\,U_{ij}a_i^*a_j^*\mathbf{a}_i \cdot \mathbf{a}_j$.

Physical measurements. Diffuse reflective UV–visible spectra over the wavelength range 190 to 900 nm were taken at room temperature on a Cary 1E spectrophotometer equipped with a diffuse reflectance accessory. Polytetrafluoroethylene powder (6 mm thick) was used as a reference. Magnetic susceptibility measurements were made at 5 kG over the temperature range 6–300 K with a Quantum Design SQUID magnetometer. Field dependency measurements were also made at 6 and 300 K and the magnetization of all samples was linearly proportional to the applied field strengths from 1 to 5 kG. All magnetic susceptibility data were corrected for core diamagnetism.

RESULTS AND DISCUSSION

Selected distances and angles for $BaErCuS_3$ and $BaYAgSe_3$ are given in Table 5. These materials crystallize in the layered $KZrCuS_3$ structure type (13) illustrated in Fig. 1 for $BaYAgSe_3$. In these structures there are two-dimensional layers $^2_\infty[LnMQ_3^{2-}]$ (M = Cu, Ag; Q = S, Se) separated by Ba^{2+} ions, which are eight-coordinate. Figure 2 shows a view of a $^2_\infty[LnMQ_3^{2-}]$ layer with the labeling scheme, while Fig. 3 shows a polyhedral representation. *Ln* atoms are coordinated by six chalcogen atoms at the

[1] See NAPS document No. 05064 for 9 pages of supplementary material. Order from ASIS/NAPS, Microfiche publications, P.O. Box 3513, Grand Central Station, New York, NY 10163. Remit in advance $4.00 for microfiche copy or $7.75 for photocopy. All orders must be prepaid. Institutions and Organizations may order by purchase order. However, there is a billing and handling charge for this service of $15. Foreign orders add $4.50 for postage and handling, for the first 20 pages, and $1.00 for additional 10 pages of material, $1.50 for postage of any microfiche orders.

TABLE 5
Selected Bond Lengths (Å) and Bond Angles (deg)

		$BaErCuS_3$	$BaYAgSe_3$
Ln–$Q(1)$	×4	2.735(2)	2.910(1)
Ln–$Q(2)$	×2	2.677(1)	2.879(1)
M–$Q(1)$	×2	2.339(2)	2.600(1)
M–$Q(2)$	×2	2.392(2)	2.624(1)
Ba–$Q(2)$	×2	3.106(2)	3.208(1)
Ba–$Q(1)$	×4	3.221(2)	3.398(1)
Ba–$Q(1)$	×2	3.470(2)	3.556(1)
$Q(1)$–Ln–$Q(1)$	×2	180	180
$Q(1)$–Ln–$Q(1)$	×2	86.41(5)	86.51(2)
$Q(1)$–Ln–$Q(1)$	×2	93.59(5)	93.49(2)
$Q(2)$–Ln–$Q(1)$	×4	89.66(5)	84.96(2)
$Q(2)$–Ln–$Q(1)$	×4	90.34(5)	95.04(2)
$Q(2)$–Ln–$Q(2)$		180	180
$Q(1)$–M–$Q(1)$		110.30(9)	110.51(4)
$Q(1)$–M–$Q(2)$	×4	108.41(4)	109.64(2)
$Q(2)$–M–$Q(2)$		112.89(10)	107.74(4)

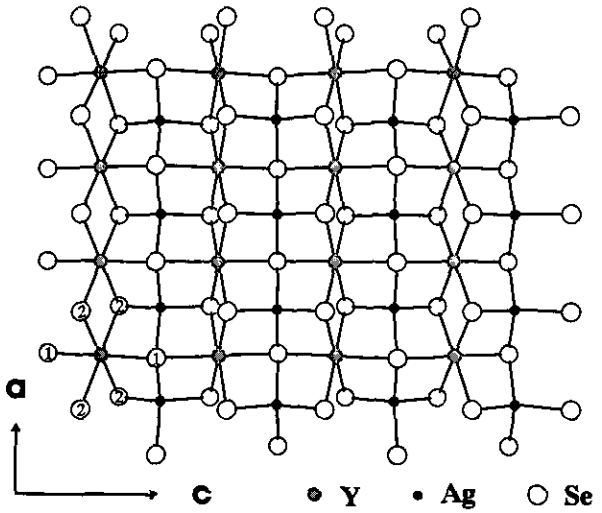

FIG. 2. View of a $^2_\infty[YAgSe_3^{2-}]$ layer along the b axis.

corners of an octahedron and M atoms are coordinated by four chalcogen atoms at the corners of a tetrahedron. In $BaErCuS_3$, the Er–S bond lengths range from 2.677(1) to 2.735(2) Å and the Cu–S bond lengths range from 2.339(2) to 2.392(2) Å. In $BaYAgSe_3$, the Y–Se bond lengths are 2.879(1) and 2.910(1) Å and the Ag–Se bond lengths are 2.600(1) and 2.624(1) Å. These values compare well with those in the literature. For example, Er–S bond lengths vary from 2.60(2) to 2.75(2) Å for the octahedrally coordinated Er atom in $CrEr_2S_4$ (19); Cu–S bond lengths vary from 2.333(2) to 2.360(2) Å in $K_3Cu_3Nb_2S_8$ (12); Y–Se bond lengths vary from 2.81(1) to 2.94(1) Å in YSeF (20); and Ag–Se bond lengths vary from 2.62(1) to 2.91(1) Å in β'-Ag_8GeSe_6 (21). In the present structures LnQ_6 octahedra share an opposite pair of edges and form chains along the a direction. The MQ_4 tetrahedra form corner-sharing chains along the a direction. The LnQ_6 chains in turn are crosslinked by sharing the two corners of each octahedron and by sharing edges with MQ_4 tetrahedra in between the octahedral chains along the c direction. The Q–M–Q (M = Cu, Ag) bond angles range from 108 to 113°.

The *Cmcm* structure adopted by $BaErCuS_3$ and $BaYAgSe_3$ is very similar to the *Pnma* structure adopted by β-$BaLaCuSe_3$, which may be viewed as a distorted version (15). The two structure types have the same atomic connectivity. In $BaErCuS_3$, all three pairs of *trans*-

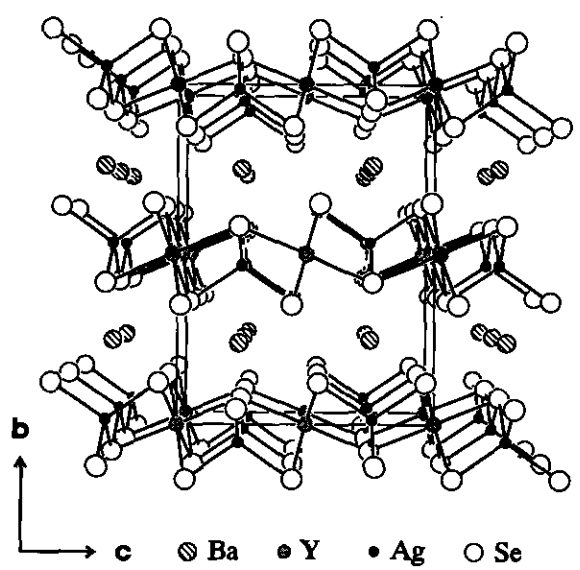

FIG. 1. Perspective view along a of the $BaYAgSe_3$ structure.

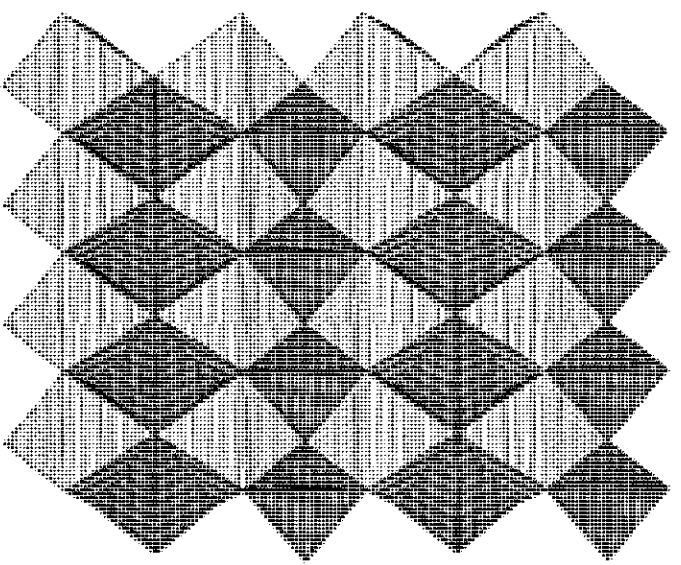

FIG. 3. A polyhedral representation of a $^2_\infty[YAgSe_3^{2-}]$ layer.

TABLE 6
Unit Cells, Space Groups, and Structure Types for the Compounds Ba$LnMQ_3$

Compound	Space group	a (Å)	b (Å)	c (Å)	V (Å^3)	Method	T (K)
$BaScCuS_3$	*Cmcm*	3.92(1)	13.32(2)	9.82(2)	513	Film	295
$BaErCuS_3$	*Cmcm*	3.987(1)	13.377(3)	10.101(2)	539	Diffractometer[b]	115
$BaYCuS_3$	*Cmcm*	4.02(1)	13.45(3)	10.19(2)	551	Film	295
$BaGdCuS_3$	*Cmcm*	4.043(2)	13.446(4)	10.287(4)	559	Powder	295
$BaNdCuS_3$	*Pmcn* (*Pnma*)	4.093(1)	13.439(4)	10.489(3)	577	Powder	295
$BaCeCuS_3$	*Pmcn* (*Pnma*)	4.125(2)	13.378(4)	10.678(3)	589	Powder	295
$BaLaCuS_3$	*Pmcn* (*Pnma*)	4.236(1)	11.724(2)	11.316(2)	562	Diffractometer[a]	115
$BaErCuSe_3$	*Cmcm*	4.15(1)	14.07(3)	10.68(2)	624	Film	295
$BaYCuSe_3$	*Cmcm*	4.19(2)	14.05(4)	10.65(2)	627	Film	295
$BaCeCuSe_3$	*Pmcn* (*Pnma*)	4.269(1)	13.903(2)	11.019(2)	654	Powder	295
β-$BaLaCuSe_3$	*Pmcn* (*Pnma*)	4.293(2)	13.830(4)	11.111(4)	660	Diffractometer[a]	115
α-$BaLaCuSe_3$	*Pmcn* (*Pnma*)	4.408(1)	12.195(2)	11.800(2)	634	Powder	295
$BaNdAgS_3$	*Cmcm*	4.187(2)	13.688(5)	10.524(4)	603	Powder	295
$BaErAgSe_3$	*Cmcm*	4.228(1)	14.037(2)	10.602(2)	629	Diffractometer	115
$BaYAgSe_3$	*Cmcm*	4.239(1)	14.030(2)	10.636(2)	633	Diffractometer[b]	115
$BaLaAgSe_3$	*Cmcm*	4.40(1)	14.34(2)	11.16(2)	704	Film	295

[a] Crystal structure determination: see Ref. (15).
[b] Crystal structure determination: this work.

Q–Ln–Q moieties in an LnQ_6 octahedron are linear; in β-$BaLaCuSe_3$ they are all bent slightly. To investigate the dependence of structure type on rare-earth metal, several other members of this series were synthesized, either as single crystals or as polycrystalline samples. For the single crystals, diffractometer or film techniques were used to determine the unit cell dimensions and systematic absences. Powder diffraction patterns from the polycrystalline samples were compared with those calculated from the known structures, as determined from single crystals. The unit cell parameters and space groups are listed in Table 6,[2] along with those for $BaErCuS_3$, $BaYAgSe_3$, $BaLaCuS_3$, and α- and β-$BaLaCuSe_3$. Figure 4 shows the room-temperature cell volume and cell edge lengths of five of these compounds of formula Ba$Ln$$CuS_3$ as a function of the radius of the Ln^{3+} ion (22). The cell volume increases with the ionic radius. For the three compounds in the space group *Cmcm* (*Ln* = Sc, Y, Gd), the cell edges vary nearly linearly with the ionic radius of Ln^{3+}. From Table 6, one can see that the $BaErCuS_3$ structure type prevails among the compounds of the smaller rare-earth elements. This is understandable because the smaller rare-earth elements tend to prefer octahedral coordination. In the compounds that contain a larger rare-earth element (Nd, Ce) as well as copper, the β-$BaLaCuSe_3$ structure type is adopted, in which chalcogen atoms are shifted so that *trans-Q–Ln–Q* angles deviate from 180°. Here the *a* and *c* axes are further lengthened while the *b* axis is shortened. Only with La, the largest rare-earth element, in α-$BaLaCuSe_3$ and $BaLaCuS_3$ does a further distortion occur, leading to collapse of the layers and to seven-coordinated La with bonds across the layers (15). Here the lengths of the *b* and *c* axes are more nearly equal.

Silver compounds are different from the corresponding copper compounds. Thus β-$BaLaCuSe_3$ and $BaNdCuS_3$ both crystallize in a *Pnma* structure, and $BaLaAgSe_3$ and $BaNdAgS_3$ crystallize in the *Cmcm* structure. This *Cmcm* structure type is also found in those selenides that contain silver and a smaller rare-earth element, e.g., $BaErAgSe_3$ and $BaYAgSe_3$. (Although the cell constants of these four silver compounds crystallizing in *Cmcm* are not plotted in Fig. 4, the monotonic change in cell dimensions with the ionic radii of the constituent elements is maintained.) However, we have found two completely different structure types in related silver systems. The compounds $Ba_2LnAg_5S_6$ (*Ln* = La, Y) crystallize in a channel structure (23). Some sulfides with smaller rare-earth elements crystallize in yet another structure type (24) unrelated to those discussed here. In this regard, an effort has been made to synthesize "$BaLaAgS_3$" by the reaction of binary sulfides. The final product consists primarily of $Ba_2LaAg_5S_6$ and $BaLa_2S_4$. If "$BaLaAgS_3$" exists, it is not stable at the reaction temperature used (850°C).

Figures 5 and 6 show the diffuse reflective UV–visible spectra of several of these compounds. A straightforward

[2] Kulakov and co-workers reported a quaternary phase with a composition (from X-ray spectral microanalysis) close to $BaYCuS_3$ in a multiphase mixture (6). They abstracted from a Debye powder pattern of a mixture of phases a cell of dimensions $a = 5.083$ and $c = 6.688$ Å and symmetry 4/*mmm* for $BaYCuS_3$. However, examination of their tabulated powder pattern reveals that with one exception (102), all indexed lines coincide in position and approximate intensity with the more intense peaks in the diffractometer powder pattern of $BaYCuS_3$ obtained in the present work. They probably obtained the present phase.

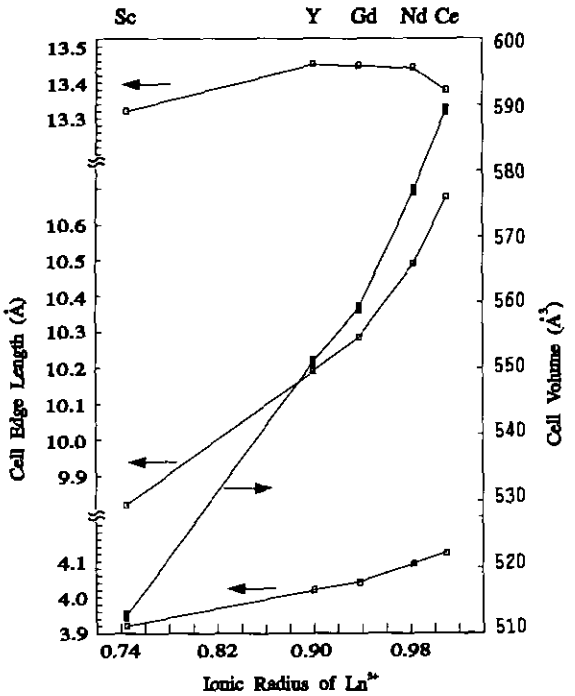

FIG. 4. Plot of the unit-cell dimensions of BaLnCuS$_3$ as a function of the ionic radius of six-coordinated Ln^{3+}.

extrapolation method (25) was used to deduce the optical band gaps. On a plot of absorbance vs photon energy, the spectrum near the absorption edge was extrapolated to the abscissa and the flat portion of the spectrum at the longer wavelength side (transparent region) was extrapolated beyond the absorption edge. The energy at the crossing point was taken as the absorption edge. The data do not enable us to carry out a detailed analysis of $\alpha h\nu$ vs $h\nu$ (26) that would provide more accurate results. Single-crystal transmission measurements are better suited for that purpose. The measured optical band gaps for four of these compounds are given in Table 7. A band gap is not given for BaCeCuS$_3$ or BaCeCuSe$_3$ because a steep region

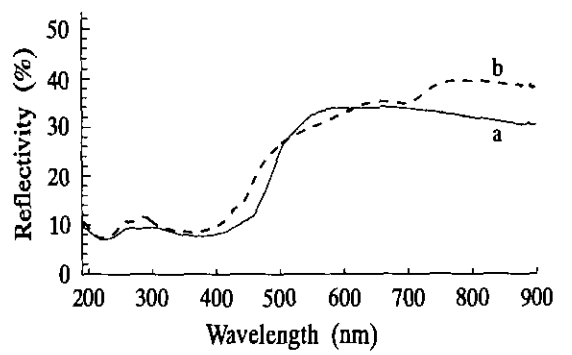

FIG. 5. Diffuse reflective UV–visible spectra of (a) BaGdCuS$_3$ and (b) BaYCuS$_3$.

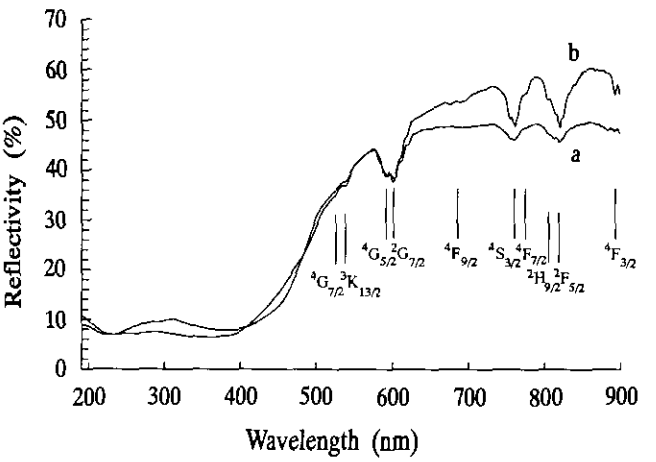

FIG. 6. Diffuse reflective UV–visible spectra of (a) BaNdCuS$_3$ and (b) BaNdAgS$_3$.

is not found in either spectrum; the spectrum of the selenide is similar to that of the sulfide but is shifted toward higher energy. In the spectra of BaNdMS$_3$ (M = Cu, Ag; Fig. 6), there are several absorption peaks at energies lower than that of the band gap. These must result from transitions associated with $4f$ electronic states as they occur at the same energies, within experimental error, as those reported for Nd^{3+} (27, 28). Over the wavelength range measured in the present work, no absorption peaks are expected for either Ce^{3+} or Gd^{3+} (27).

Plots of the reciprocal molar magnetic susceptibilities of BaNdCuS$_3$ and BaGdCuS$_3$ as a function of temperature are shown in Fig. 7, and those of BaCeCuS$_3$ and BaCeCuSe$_3$ are shown in Fig. 8. These data have been fit to the expression $\chi = C/(T - \theta) + \chi_0$, where χ_0 is the Van

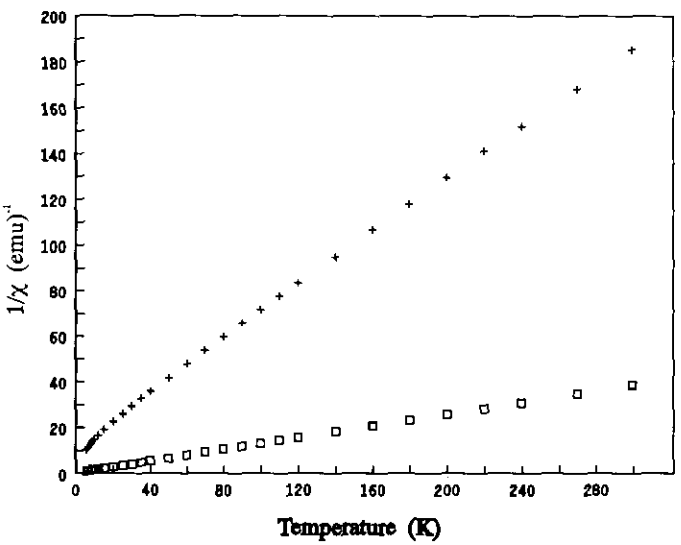

FIG. 7. Measured magnetic susceptibilities of BaNdCuS$_3$ (+) and BaGdCuS$_3$ (□).

TABLE 7
Optical and Magnetic Results for Several Ba$LnMQ_3$ Compounds

Compound	Sample color	Band gap (eV)	C^a (emu · K/mole)	θ^a (K)	$\chi_0{}^a$ (emu/mole)	μ_{eff} at 300 K (B.M.)
$BaYCuS_3$	Yellow orange	2.61(3)				
$BaNdCuS_3$	Yellow green	2.39(3)	1.03(4)	−5.3(4)	0.0036(5)	3.60(1)
$BaNdAgS_3$	Yellow green	2.31(4)				
$BaGdCuS_3$	Yellow green	2.41(3)	7.95(2)	−1.6(1)	−0.0012(4)	7.88(1)
$BaCeCuS_3$	Green		0.212(2)	−1.5(1)	0.00240(3)	2.60(2)
$BaCeCuSe_3$	Dark green		0.219(4)	−1.0(2)	0.00239(8)	2.54(2)

[a] Data fit to the formula $\chi = C/(T - \theta) + \chi_0$.
[b] $\mu_{eff} = (3kT\chi/N\beta^2)^{1/2}$. β is the Bohr magneton.

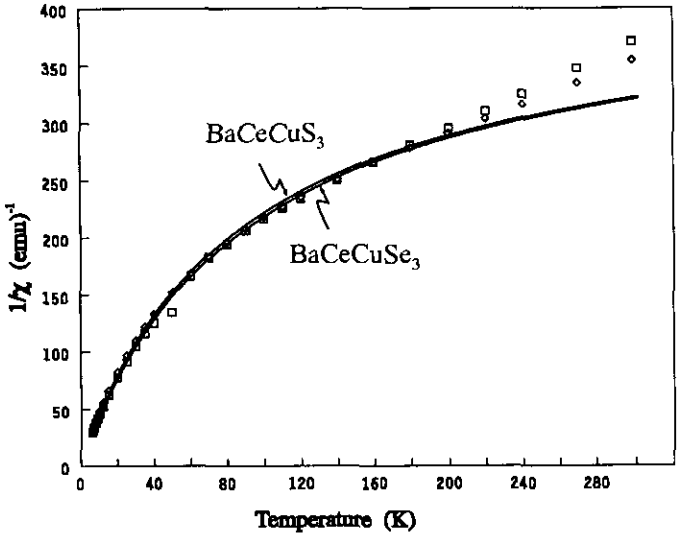

FIG. 8. Measured magnetic susceptibilities of $BaCeCuS_3$ (◇) and $BaCeCuSe_3$ (□). The solid lines are the result of fitting the data to the expression $\chi = C/(T - \theta) + \chi_0$.

Vleck temperature-independent paramagnetic susceptibility. The resultant parameters are given in Table 7. Both $BaNdCuS_3$ and $BaGdCuS_3$ essentially follow the Curie–Weiss law, while $BaCeCuS_3$ and $BaCeCuSe_3$ display, in addition, temperature-independent paramagnetism. The effective Bohr magneton numbers at room temperature are also listed in Table 7. These values are consistent with the theoretical values for the corresponding Ln^{3+} ions (29).

ACKNOWLEDGMENTS

Use was made of the X-ray, scanning electron microscope, and magnetic susceptibility facilities supported by the National Science Foundation through the Northwestern University Materials Research Center, Grant DMR91-20521. This research was supported by the National Science Foundation through Grant DMR91-14934.

REFERENCES

1. J. Flahaut, *in* "Handbook on the Physics and Chemistry of Rare Earths, Vol. 4" (K. A. Gschneidner, Jr. and L. R. Eyring, Eds.), p. 1. North-Holland, Amsterdam/New York/Oxford, 1979.
2. A. A. Eliseev, O. A. Sadovskaya, and G. M. Kuz'micheva, *Inorg. Mater. Engl. Transl.* **18,** 1435 (1982).
3. R. Ibañez, A. Garcia, C. Fouassier, and P. Hagenmuller, *J. Solid State Chem.* **53,** 406 (1984).
4. J. A. Savage and K. L. Lewis, *Proc. SPIE-Int. Soc. Opt. Eng* **683** 79 (1986).
5. R. Ithnin, D. J. Gilbert, S. Arnold, and J. V. Acrivos, *NATO ASI Ser., Ser. B* **172** 507 (1987).
6. M. P. Kulakov, S. A. Zver'kov, V. K. Gartman, N. N. Kolesnikov, O. V. Zharikov, and G. I. Peresada, *Inorg. Mater. Engl. Trans.* **27,** 1653 (1992).
7. R. Ibanez, P. Gravereau, A. Garcia, and C. Fouassier, *J. Solid State Chem.* **73,** 252 (1988).
8. J. D. Carpenter and S.-J. Hwu, *Chem. Mater.* **4,** 1368 (1992).
9. Y.-J. Lu and J. A. Ibers, *J. Solid State Chem.* **94,** 381 (1991).
10. Y.-J. Lu and J. A. Ibers, *Inorg. Chem.* **30,** 3317 (1991).
11. P. Wu, Y.-J. Lu, and J. A. Ibers, *J. Solid State Chem.* **97,** 383 (1992).
12. Y.-J. Lu and J. A. Ibers, *J. Solid State Chem.* **98,** 312 (1992).
13. M. F. Mansuetto, P. M. Keane, and J. A. Ibers, *J. Solid State Chem.* **101,** 257 (1992).
14. P. Wu and J. A. Ibers, *Acta Crystallogr., Sect. C: Cryst. Commun.* **49,** 126 (1993).
15. A. E. Christuk, P. Wu, and J. A. Ibers, *J. Solid State Chem.* **110,** 330 (1994).
16. J. C. Huffman, unpublished work.
17. G. M. Sheldrick, SHELXTC PC Version 4.1, An Integrated System for Solving, Refining, and Displaying Crystal Structures from Diffraction Data. Siemens Analytical X-Ray Instruments, Inc., Madison, WI.
18. G. M. Sheldrick, SHELXL-92 Unix Beta-test version.
19. A. Tomas, R. Chevalier, P. Laruelle, and B. Bachet, *Acta Crystallogr., Sect. B: Struct. Crystallogr. Cryst. Chem.* **32,** 3287 (1976).
20. Nguyen-Huy-Dung and P. Laruelle, *Acta Crystallogr., Sect. B: Struct. Crystallogr. Cryst. Chem.* **33,** 3360 (1977).
21. D. Carré, R. Ollitrault-Fichet, and J. Flahaut, *Acta Crystallogr., Sect. B: Struct. Crystallogr. Cryst. Chem.* **36,** 245 (1980).
22. R. D. Shannon, *Acta Crystallogr., Sect. A: Cryst. Phys. Diffr. Theor. Gen. Crystallogr.* **32,** 751 (1976).
23. P. Wu and J. A. Ibers, *Z. Kristallogr.* **208,** 35 (1993).

24. P. Wu and J. A. Ibers, *J. Solid State Chem.*, in press.
25. O. Schevciw and W. B. White, *Mater. Res. Bull.* **18,** 1059 (1983).
26. T. P. McLean, *in* "Progress in Semiconductors, Vol. 5" (A. F. Gibson, Ed.), p. 53. Wiley, New York, 1960.
27. S. Cotton, "Lanthanides and Actinides," p. 29. Oxford Univ. Press. New York, 1991.
28. J. R. Henderson, M. Muramoto, J. B. Gruber, and R. Menzel, *J. Chem. Phys.* **52,** 2311 (1970).
29. J. H. Van Vleck, "The Theory of Electric and Magnetic Susceptibilities." Oxford Univ. Press, London, 1932.
30. J. C. Huffman, Ph.D. thesis, Indiana University, 1974.
31. J. de Meulenaer and H. Tompa, *Acta Crystallogr.* **19,** 1014 (1965).